Available online at www.sciencedirect.com

SciVerse ScienceDirect

Geochimica et Cosmochimica Acta 118 (2013) 18–32

Geochimica et Cosmochimica Acta

www.elsevier.com/locate/gca

Experimental determination of equilibrium magnesium isotope fractionation between spinel, forsterite, and magnesite from 600 to 800 °C

Catherine A. Macris *, Edward D. Young, Craig E. Manning

Department of Earth and Space Sciences, University of California at Los Angeles, Los Angeles, CA 90095-1567, USA

Received 30 January 2013; accepted in revised form 5 May 2013; Available online 14 May 2013

Abstract

Magnesium isotopes are potentially powerful tracers for high-temperature geochemical processes if relevant fractionation factors are known. However, experimental data for Mg isotope fractionation are lacking at high temperatures. We performed experiments at 600, 700, and 800 °C and 1 GPa to establish the equilibrium magnesium isotope partitioning between forsterite (Mg_2SiO_4) and magnesite ($MgCO_3$) and between spinel ($MgAl_2O_4$) and magnesite, making use of the carbonate as an isotope exchange medium to overcome sluggish diffusion-limited magnesium isotope exchange between spinel and forsterite. Using the three-isotope method, the magnitudes of exchange between forsterite and magnesite, and between spinel and magnesite, were determined at the three temperatures for varying lengths of time, allowing equilibrium isotope partitioning to be established. Results are as follows: $\Delta^{26}Mg_{Fo-Mgs} = 0.04 \pm 0.04‰$ at 800 °C, $0.11 \pm 0.10‰$ at 700 °C, and $0.44 \pm 0.10‰$ at 600 °C; and $\Delta^{26}Mg_{Spl-Mgs} = 0.90 \pm 0.28‰$ at 800 °C, $1.10 \pm 0.27‰$ at 700 °C, and $1.73 \pm 0.38‰$ at 600 °C. From these experimentally determined equilibrium fractionation values, we derive the temperature-dependent equilibrium fractionation between spinel and forsterite by difference, yielding $\Delta^{26}Mg_{Spl-Fo}$ values of $0.86 \pm 0.29‰$ at 800 °C, $0.99 \pm 0.29‰$ at 700 °C, and $1.29 \pm 0.39‰$ at 600 °C. These data agree well with first-principles estimates of equilibrium magnesium isotope fractionation between spinel and forsterite at high temperatures. The data allow the calculation of an experimentally determined equation for the temperature dependence of $^{26}Mg/^{24}Mg$ fractionation between spinel and olivine: $\Delta^{26}Mg_{Spl-Fo} = 0.96(\pm 0.21) \times 10^6/T^2$. This first high-$T$ experimental calibration of Mg isotope fractionation of mantle minerals is consistent with expectations based on the crystal chemical environment of Mg in these phases.
Published by Elsevier Ltd.

1. INTRODUCTION

The use of non-traditional stable isotopes (i.e., stable isotopes of elements heavier than H, C, N, O, S) is rapidly growing as a tool in geochemistry because multiple-collector inductively-coupled plasma-source mass spectrometry (MC-ICPMS) allows for measuring the high-temperature partitioning of isotopes of some of the heavier rock-forming elements, including iron, silicon, magnesium, calcium, and nickel. Recent studies have used this tool to measure small, but significant, fractionations of iron and magnesium isotopes between minerals in mantle xenoliths (e.g., Williams et al., 2009; Young et al., 2009; Huang et al., 2011). Comparisons of published inter-mineral isotope fractionation data with quantitative predictions are in some cases consistent with theory, but in other cases not. It is therefore essential to compare measurements of stable isotope fractionation in natural samples and theoretical predictions with experimental evidence wherever possible. Experimental studies to date have focused on iron, silicon, and nickel isotope fractionation between minerals at high temperatures (e.g., Shahar et al., 2008, 2011; Lazar et al., 2012).

* Corresponding author. Current address: Division of Geological and Planetary Sciences, California Institute of Technology, Pasadena, CA 91125, USA.

E-mail addresses: camacris@caltech.edu, cmacris@ucla.edu (C.A. Macris).

0016-7037/$ - see front matter Published by Elsevier Ltd.
http://dx.doi.org/10.1016/j.gca.2013.05.008

This study provides the first experimental data for magnesium isotope fractionation between minerals at high T–P conditions.

The lack of data on Mg isotope fractionation at high temperatures limits use of this system for petrogenetic interpretation. For example, the degree of isotopic equilibrium or lack thereof between minerals of a major rock-forming element like Mg can be used to sort out parageneses in rocks with complex histories (e.g., Young et al., 2009). While recent contributions have expanded the limited data for Mg fractionation in naturally occurring mantle minerals (e.g., Wiechert and Halliday, 2007; Handler et al., 2009; Yang et al., 2009; Young et al., 2009; Chakrabati and Jacobsen, 2010; Liu et al., 2011; Huang et al., 2011), they have also served to highlight the complexity of isotopic relationships in these rocks that can only be understood with well-established equilibrium inter-mineral fractionation factors. Comparisons of theoretical predictions of inter-mineral Mg isotope fractionations by Schauble (2011) with spinel–olivine fractionation measurements from mantle xenolith samples in the current data set yield mixed results. Data from Young et al. (2009) agree (within error) with predictions for spinel–forsterite Mg fractionation both qualitatively (on the basis of Mg coordination environments) and quantitatively. Data for this same mineral pair presented by Liu et al. (2011) define smaller fractionations than theoretical predictions by several tenths of per mil. The authors argue that this discrepancy is due in part to the effect of cation substitution in spinel, but theoretical estimates for the effects of cation substitution on spinel–olivine fractionation alone are not sufficient to explain the deviations from theory. This ambiguity highlights the need for experimental calibrations of inter-mineral Mg isotope fractionation, especially between spinel and olivine where fractionations are large due to the different coordination environments for Mg in these phases.

It is also important to understand the isotope fractionation between Mg-bearing carbonates such as magnesite and other phases. Magnesian carbonate may be a major CO_2 reservoir in the upper mantle (e.g., Katsura and Ito, 1990) and determining the degree to which occurrences of mantle carbonate are in Mg isotopic equilibrium with surrounding rock may prove useful in establishing the provenance of the carbonate. Several studies have investigated Mg isotope fractionations associated with carbonate precipitation and dissolution in aqueous solutions at low temperatures (e.g., Galy et al., 2002; Wombacher et al., 2006). However, it is not clear whether the experiments in these studies represent equilibrium or kinetic fractionations. Young and Galy (2004) showed that kinetic isotope effects likely contribute to the low $^{26}Mg/^{24}Mg$ seen in some carbonate precipitates in nature.

The kinetic vs. equilibrium isotopic fractionation in carbonates is an important issue that has been the topic of several recent experimental studies. Experiments by Mavromatis et al. (2011) demonstrate that Mg isotope fractionation between magnesite and fluid at low temperatures depends on precipitation rates and the concentration of aqueous organic ligands. They conclude that these factors may be responsible in part for the degree of Mg isotopic fractionation observed in nature. Pearce et al. (2012) found that Mg isotope exchange between magnesite and fluid displays both kinetic and equilibrium behaviors, but concluded that the kinetic signal would be eradicated by equilibrium fractionation in most natural samples. Both of these studies were based on experiments at low temperatures and involved fractionations between magnesite and aqueous liquid associated with precipitation and/or dissolution. New experiments are needed to determine the equilibrium fractionation of magnesium isotopes between carbonates and other minerals at high temperatures where kinetic limitations are more easily circumvented; high-temperature experiments offer a means to separate the potentially confusing kinetic isotope signals from those representing equilibrium among co-existing minerals in nature.

In this study we use the three-isotope exchange method (Matsuhisa et al., 1978) to determine experimentally the equilibrium magnesium isotope fractionation factors between forsterite (Fo) and magnesite (Mgs), and between spinel (Spl) and magnesite as a function of temperature. Making use of the well-established advantages of using carbonate as an exchange medium and exchange partner (e.g., Clayton et al., 1989; Chacko et al., 1996), we achieved significant exchange of Mg isotopes between the two mineral pairs, Spl–Mgs and Fo–Mgs, at a range of temperatures. These experiments resulted in the direct determination of equilibrium Mg isotope fractionation between spinel and magnesite, and between forsterite and magnesite, which, when combined, allows for the determination of the equilibrium fractionation between spinel and forsterite.

2. METHODS

2.1. The three-isotope method combined with the use of carbonate as an exchange medium

The three-isotope technique was first used by Matsuhisa et al. (1978) to obtain equilibrium fractionation factors for oxygen isotopes between quartz and water. Shahar et al. (2008) first applied the method to obtain isotope fractionation between two solid phases by investigating Fe-isotope exchange between magnetite and fayalite. Subsequent studies have employed the technique to determine high temperature equilibrium fractionation factors between solids for Si and Ni (e.g., Shahar et al., 2009, 2011; Lazar et al., 2012). Here we present a brief review of the method and describe how it was employed in the current study by utilizing carbonate as an exchange medium.

A schematic representation of the three-isotope method is shown in Fig. 1. A three-isotope plot consists of two axes defined by two isotope ratios with the same denominator. The present study utilizes changes in $^{25}Mg/^{24}Mg$ and $^{26}Mg/^{24}Mg$ ratios relative to a standard reported in per mil (‰). The per mil deviations are expressed in conventional delta notation:

$$\delta^i\mathrm{Mg} = 10^3\left(\frac{(^i\mathrm{Mg}/^{24}\mathrm{Mg})_{\mathrm{Sample}}}{(^i\mathrm{Mg}/^{24}\mathrm{Mg})_{\mathrm{Standard}}} - 1\right) \quad (1)$$

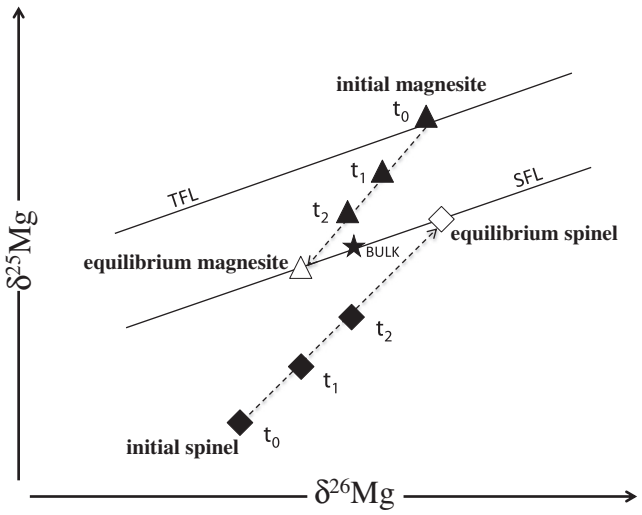

Fig. 1. Schematic diagram of the three-isotope exchange method showing the terrestrial fractionation line (TFL) where natural samples lie, and the secondary fractionation line (SFL) that has the same slope as the TFL but is offset due to a ^{24}Mg spike affecting the bulk composition of the system. The intersections of the trend lines from the experiments with the SFL define equilibrium isotopic compositions. See text for further explanation.

where $i = 25$ or 26. The goal is to derive the equilibrium isotope distribution by extrapolation to the condition of isotopic equilibrium defined by the mass fractionation relationship between the two isotope ratios of interest. Cast in terms of magnesium isotopes the relationship is:

$$\delta^{25}\mathrm{Mg} = (10^3 + \delta^{25}\mathrm{Mg}_{\mathrm{bulk}})\left(\frac{10^3 + \delta^{26}\mathrm{Mg}}{10^3 + \delta^{26}\mathrm{Mg}_{\mathrm{bulk}}}\right)^{\gamma} - 10^3 \qquad (2)$$

In Eq. (2) all delta values are relative to the same standard. For our purposes, the slightly concave fractionation relationship in Eq. (2) can be approximated by a straight line in three-isotope space with a slope of approximately γ and an intercept defined by the isotopic composition labeled bulk (or any point on the fractionation curve). The exponent, γ, is taken to be 0.521 at equilibrium based on the expression for equilibrium mass fractionation,

$$\gamma = \frac{\left(\frac{1}{m_{24}} - \frac{1}{m_{25}}\right)}{\left(\frac{1}{m_{24}} - \frac{1}{m_{26}}\right)} \qquad (3)$$

where m_i is the precise mass of each isotope i. Equilibrium isotopic compositions in a system with a specified bulk isotopic composition fall on the fractionation curve (or line) defined by Eq. (2). In the three-isotope method, starting compositions lie off the final fractionation curve, and progress towards this line as they move towards equilibration. In Fig. 1, one of the starting phases is "normal", in that it has a natural isotope value and plots on the terrestrial fractionation line (TFL). The other starting phase is "spiked" with a known amount of the denominator isotope for both axes (in this case ^{24}Mg), thereby displacing it from the TFL in three-isotope space along a line with a slope of unity. A series of experiments is performed on mixtures of two starting materials with constant proportions at the same high T–P conditions, but for varying lengths of time. During the experiments, isotopes exchange between phases, resulting in lines defined by the isotopic compositions of the two starting phases and the equilibrium compositions of the two phases. The equilibrium compositions must lie on the secondary fractionation line (SFL) defined by the bulk composition of the mixture of starting compositions (Fig. 1).

A distinct advantage of this approach is that the two phases need not reach equilibrium during the experiments. The isothermal time-series are linear (Lazar et al., 2012), permitting extrapolation of each time series to the SFL and therefore the equilibrium isotopic compositions (Eq. (2)). In this way, the equilibrium isotopic compositions of each phase are obtained by the intersections of the lines defined by the time series for that phase and the SFL (Fig. 1). The difference between these extrapolated intersections is the equilibrium inter-mineral fractionation value at a given temperature, e.g., for the present study:

$$\Delta^{26}\mathrm{Mg}_{\mathrm{Spl–Mgs}} = \delta^{26}\mathrm{Mg}_{\mathrm{Spl}} - \delta^{26}\mathrm{Mg}_{\mathrm{Mgs}} \qquad (4)$$

where $\delta^{26}\mathrm{Mg}_{\mathrm{Spl}}$ is equal to the value of the open circle in Fig. 1 and $\delta^{26}\mathrm{Mg}_{\mathrm{Mgs}}$ is equal to the value of the open triangle.

The linear extrapolation from the $\delta^{26}\mathrm{Mg}_{\mathrm{Spl}}$ and $\delta^{26}\mathrm{Mg}_{\mathrm{Mgs}}$ values representing a time series (Fig. 1, t_0–t_2) is obtained from the weighted linear regression algorithm of Mahon (1996). Following Shahar et al. (2008), the uncertainties in the slopes and intercepts of the regression analyses are used to calculate uncertainties in fractionation factors. Errors and their propagations are discussed in greater detail in Section 2.5.

There are two requirements for successful determination of equilibrium fractionation factors with the three-isotope method: (1) varying degrees of isotope exchange must be achieved between phases of interest during the experiments, and (2) all phases containing the isotopes of interest must

be completely separated after the experiments for analysis. In past studies involving mineral–mineral exchange, the first requirement was met by utilizing heterogeneous reactions to promote isotope exchange. For example, Shahar et al. (2009) forced iron isotope exchange between fayalite and magnetite as a function of temperature in the assemblage magnetite + quartz + fayalite comprising the "QFM" oxygen fugacity buffer. Lazar et al. (2012) also used heterogeneous reaction to promote Ni isotope exchange between Ni-metal and Ni-talc by converting spiked NiO to Ni-talc at high T–P, leading to a final assemblage of metal + talc + quartz + H_2O. However, the phases involved in the Mg system are substantially more refractory and therefore pose challenges for this approach.

The second requirement for successful application of the three-isotope method, complete separation of run products containing the specified isotope(s), is an equally important part of the experiment. Significant contamination of either phase with the other would result in spurious fractionation factors. Both Shahar et al. (2008) and Lazar et al. (2012) were able to separate their run products with a strong magnet because one of the phases of interest in their final assemblages was magnetic, while the other phase was not. None of the phases of interest in this study are magnetic.

We solved the twin problems of refractory compounds and difficulty of separation by utilizing magnesite as both an exchange medium for Mg isotopes and an exchange partner for both spinel and forsterite. Exploratory runs indicated significant isotopic exchange. And, by taking advantage of the high solubility of magnesite in warm HCl, we were able to preferentially dissolve the magnesite after each experiment, allowing for complete separation of phases for analyses. The specifics of our experimental methods are discussed in the following sections.

2.2. Piston–cylinder experiments

Starting materials were finely ground powders of synthetic, high-purity forsterite, spinel, and anhydrous magnesite. Forsterite and spinel were both synthesized by combining stoichiometric amounts of ultrapure powders of $MgO + SiO_2$ and $MgO + Al_2O_3$ (Alfa Aesar), respectively. The MgO component of both mixtures was spiked with excess ^{24}Mg by mixing the ultrapure MgO (Alpha Aesar) with high-purity α-^{24}MgO (Oak Ridge National Laboratory Batch 217101, ^{24}Mg 99.92%, ^{25}Mg 0.05%, ^{26}Mg 0.03%) in a ~99:1 ratio, ground twice under acetone in a mortar and pestle for ~30 min.

Reactant forsterite was synthesized from a stoichiometric mixture of SiO_2 powder + spiked MgO powder homogenized by grinding in a mortar and pestle. The ground mixture was devolatilized in a platinum crucible at 800 °C for approximately 120 min, cooled, and finely ground again in an agate mortar and pestle. The material was then pelletized and sintered in an upright furnace at 1400 °C for 72 h, resulting in >99% pure forsterite as determined by X-ray diffraction. For spinel synthesis, the stoichiometric Al_2O_3 + spiked MgO was homogenized and devolatilized in the same manner as the forsterite. The spinel was grown from the powdered oxide mix hydrothermally in a piston–cylinder apparatus. Anhydrous synthetic magnesite was purchased from Sargent–Welch. Magnesium isotope compositions of starting materials are given in Table 1.

For each experiment two separate capsules were made: one containing forsterite + magnesite, and one containing spinel + magnesite, both with approximately 1:1 M Mg proportions. To make the capsules, starting assemblages were loaded into segments of Au tubing of 3.5 mm outer-diameter and 0.18 wall thickness. After loading, the tubes were sealed by welding with a carbon electrode, and the sealed capsules were loaded side by side into a 1-in. diameter piston–cylinder assembly with NaCl pressure medium and graphite heater sleeve. A thin piece of Au was placed on top of the capsules to prevent puncture by the thermocouple. Temperature was monitored with $Pt/Pt_{90}Rh_{10}$ thermocouples in contact with the capsules, with no correction for the effect of pressure on emf (Ulmer, 1971). The accuracy of the reported temperature is estimated to be ±3 °C. All experiments were brought to a pressure of 7 kbar and then heated to the desired run temperature at a rate of ~20 °C per minute. As the assembly heated, thermal expansion of the assembly brought the pressure to 10 kbar. Pressure was monitored with a Heise Bourdon-tube pressure gauge and maintained to within 200 bar gauge pressure. Experiments were performed at 600–800 °C for 15–240 min. Runs were quenched by cutting power to the apparatus, which resulted in cooling of the experiment to <50 °C in <1 min (Manning and Boettcher, 1994). Following each run, the capsules were retrieved, cleaned, and weighed. They were then opened with a clean razor blade and run products were transferred to glass containers.

2.3. Sample separation and purification

The starting assemblages of the spinel–magnesite (Spl–Mgs) and forsterite–magnesite (Fo–Mgs) experimental charges were loaded into the Au capsules as loose microscopic powders. The post-run products were re-crystallized to various extents, but crystals were still too small and intermingled to be quantitatively separated by hand. Complete separation of run products was achieved by developing a procedure for the preferential dissolution of magnesite.

Run products were transferred into Savillex vials and 1 ml of warm (~150 °C) 1 N HCl was added. The vials were sonicated for ~5 min, then centrifuged for ~2 min to separate the remaining solids from the liquid which now contained dissolved magnesite. The supernatant fluid was then carefully pipetted into a separate Savillex vial through filter paper (to exclude any crystals that might be pipetted off accidentally). This procedure was repeated 3 times with warm HCl, then twice more with room temperature Millipore H_2O. The supernatant fluid portion from this procedure, which now contains only dissolved magnesite from the run, is dried at 120 °C, redissolved in aqua regia, dried again, then picked up in 2% HNO_3 for mass spectrometry. The leftover solids in the vial, which were >95% forsterite or spinel, were also dried at 120 °C.

Table 1
Mean isotopic compositions of experimental starting materials for each isothermal time series. δ values are reported relative to Spex 3 for 700 °C experiments, and Spex 4 for 600 and 800 °C experiments. Uncertainties reflect internal precision for measurements.

	Starting mineral	δ^{25}Mg (‰)	2se	δ^{26}Mg (‰)	2se
800 °C	Forsterite	−12.744	0.008	−13.147	0.009
	Spinel	−12.842	0.013	−13.544	0.050
	Magnesite	1.792	0.012	3.404	0.011
700 °C	Forsterite	−10.844	0.010	−11.700	0.022
	Spinel	−13.419	0.042	−14.576	0.040
	Magnesite	1.0058	0.034	1.928	0.012
600 °C	Forsterite	−12.744	0.008	−13.147	0.009
	Spinel	−12.842	0.013	−13.544	0.050
	Magnesite	1.792	0.012	3.404	0.011

We tested the integrity of this procedure by applying it to mixtures of isotopically spiked spinel + terrestrial magnesite and spiked forsterite + terrestrial magnesite (similar to the starting assemblages of the exchange experiments). Both mixtures underwent the preferential dissolution procedure as described above, their respective separates were then dissolved, and in the case of spinel, put through Mg purification columns (as described below). Each separate was then analyzed by MC-ICPMS and found to be identical (within error of analysis) to measured values of original starting materials that did not undergo the preferential dissolution procedure, thus proving the successful separation of phases. Based on the precision of the isotope ratio analysis, the maximum intermingling of Mg from this procedure is ~5%.

Forsterite and spinel crystals from all experiments were dissolved in sealed Teflon® vessels jacketed in steel acid digestion bombs (Parr Instrument Co.) in a 1:1 mixture of omnigrade HF and HNO_3 at temperatures of 230 °C for 72 h. Dissolved samples were transferred to Savillex vials and evaporated to dryness at 120 °C. Dried samples were redissolved in aqua regia at 120 °C for 24 h followed by evaporation to dryness. Forsterite samples were then dissolved again in 2% HNO_3 for mass spectrometry. Spinel samples were redissolved in 1 N HNO_3 in preparation for ion exchange column chemistry.

Magnesium from spinel was purified by ion exchange chromatography in HEPA® filtered laminar flow boxes within a class 100 clean laboratory using a one-column procedure modified from Young et al. (2009). We used PFA micro-columns measuring 120 mm × 4 mm with 70 ml reservoirs. These columns contain 1.5 ml (wet) of Bio-Rad™ AG 50W-X12 resin in 200–400 mesh hydrogen form. The 2.1 meq capacity of the resin translates to a column capacity of 36 mg Mg^{2+}. Columns were washed initially with 0.5 N HF followed by a rinse with ~18 MΩ cm^2/cm water, cleaning with 6 N HCl, and further rinsing. Resins were conditioned with 1 N HNO_3. A typical load on the column consists of between ~50 μg of Mg in 300 μl of 1 N HNO_3. This column is used to separate Mg from Al by eluting Mg with 70 ml of 1 N HNO_3. Recovered magnesium is again evaporated to dryness, then redissolved in 2% HNO_3 for mass spectrometry. Repeating this entire procedure, from dissolution to purification on two different aliquots of our synthetic spinel starting material, results in an external reproducibility of ±0.05 (2 SD).

The most reliable indicator of complete recovery of Mg in the presence of matrix elements on the columns was the absence of measurable shifts in $^{25}Mg/^{24}Mg$ and $^{26}Mg/^{24}Mg$ following Mg recovery. These "zero enrichments" were checked for in-house reference Mg upon each load of resin. Blanks of Mg were below detection. Forsterite and magnesite samples did not go through this column chemistry procedure because the dissolution procedure alone served to purify Mg.

2.4. Mass spectrometry

All Mg isotope ratio measurements were made using a Thermo-Finnigan Neptune MC-ICPMS. The instrument has a fixed array of 9 Faraday collectors each with amplifier resistors of 10^{11} Ω. Sample purity was checked by monitoring $^{27}Al^+$, $^{44}Ca^+$, $^{52}Cr^+$, $^{55}Mn^+$ and $^{56}Fe^+$. In all cases the abundances of these potential impurities were <1 at.% of the analyte Mg concentration. Such low impurity/Mg ratios are well below thresholds for discernible matrix effects on Mg isotope ratio measurements as determined by tests using various mixtures of these elements under our operating conditions. Samples and standard were analyzed as ~2 ppm Mg in 2% HNO_3 aspirated through a Cetac Aridus II® desolvating nebulizer (samples were run in dry plasma) with addition of N_2. Potential mass interferences from C_2^+ and CN^+ (below detection) were resolved from $^{24}Mg^+$ and $^{26}Mg^+$, respectively, by operating at a high mass resolving power of >10,000 ($m/\Delta m$ as measured on the off-axis major beam peak shape). Samples were analyzed 8–13 times with each analysis consisting of 20 cycles of ~4 s integrations. Corrections for instrumental mass bias were obtained by sample-standard bracketing with peak height matching between sample and standard to better than 5%. Uncertainties for each datum are reported as 2 standard errors (2se), representing the uncertainty in the mean from the mass spectrometry blocks of 20 cycles.

In this study it is the relative differences in Mg isotope ratios that are of interest. All values for Mg isotope ratios presented in this study were obtained by using Spex CertiPrep™ Mg concentration standard solutions for our internal standard. All data are presented in the conventional

delta notation (Eq. (1)). Over the course of these experiments, we consumed all of our initial standard solution (Mg Spex 3), and were forced to switch to a new bottle (Mg Spex 4). Therefore one should not make direct comparisons of the $\delta^{25}Mg$ and $\delta^{26}Mg$ values from the 700 °C experiments with those of the 600 and 800 °C experiments. This does not affect the final determination of equilibrium fractionation because it is the relative differences between delta values in an experimental series, not the absolute measured values, that matter when determining fractionation between phases at a given temperature. We did not convert our internal standard values to the DSM3 scale because this incurs an additional systematic error (in the form of uncertainties in the isotopic compositions of Spex 3 and Spex 4 relative to DSM3) that could degrade the quality of the derived fractionation factors. Conversions from Spex 3 and Spex 4 to DSM3 scale can be made using the following values: $\delta^{25}Mg^{Spex3/DSM3} = -1.0533 \pm 0.0077$, $\delta^{26}Mg^{Spex3/DSM3} = -2.0605 \pm 0.0068$, $\delta^{25}Mg^{Spex4/DSM3} = -1.7992 \pm 0.0053$, $\delta^{26}Mg^{Spex4/DSM3} = -3.4874 \pm 0.0045$. Using these measured values, we obtain $\delta^{25}Mg^{Spex3/Spex4} = 0.747$.

2.5. Analytical errors and their propagation

Uncertainties in $\Delta^{26}Mg_{Fo-Mgs}$ and $\Delta^{26}Mg_{Spl-Mgs}$ reported in this study are derived from isotope ratio measurements of multiple forsterite and magnesite pairs, and multiple spinel and magnesite pairs, respectively. The method of propagating the uncertainties in individual analyses to the final equilibrium value is the same as that used by Shahar et al. (2008) for iron isotopes, and is described below for our magnesium isotope experiments.

The uncertainty in each isotope ratio measurement is the standard error of 8–13 MC-ICPMS analyses of the same sample solution. These analyses represent mineral separates from each experiment run at specific temperatures and times. Analyses of a given mineral representing an isothermal time series are regressed using a York regression (Mahon, 1996), resulting in a best fit line and associated uncertainties in slope and intercept for each mineral from the experimental time series. The equilibrium $\Delta^{26}Mg_{Fo-Mgs}$ and $\Delta^{26}Mg_{Spl-Mgs}$ for that temperature are obtained from the difference in the intersection of the forsterite (or spinel) and magnesite regression lines with the secondary fractionation line in three-isotope space using the relation

$$\delta^{26}Mg_{Eq,i} = \frac{-b_1 + b_2}{m_1 - \gamma} \quad (5)$$

where $\delta^{26}Mg_{Eq,i}$ is the projected $\delta^{26}Mg$ value for mineral i at equilibrium, m_1 is the slope of the regressed data points for mineral i, γ is the slope of the secondary fractionation line, b_1 is the intercept of the best-fit line through the regressed data points, and b_2 is the intercept of the secondary fractionation line.

Uncertainties in the derived $\Delta^{26}Mg_{Fo-Mgs}$ and $\Delta^{26}Mg_{Spl-Mgs}$ values are obtained from the intersections of the 2σ error envelopes for the forsterite (or spinel) and magnesite best-fit lines with the secondary fractionation line. The $\delta^{26}Mg$ values for the intersection of the SFL and the error envelope for each best-fit line are calculated as in Shahar et al. (2008). Standard errors for the equilibrium $\delta^{26}Mg$ values obtained for forsterite, spinel, and magnesite are then propagated through to the final $\Delta^{26}Mg_{Fo-Mgs}$ and $\Delta^{26}Mg_{Spl-Mgs}$ by summing the uncertainties for the two extrapolated $\delta^{26}Mg_{Eq,i}$ values in quadrature.

The $\Delta^{26}Mg_{Spl-Fo}$ values at each temperature were calculated from the difference between $\Delta^{26}Mg_{Spl-Mgs}$ and $\Delta^{26}Mg_{Fo-Mgs}$ determined by experiments. The uncertainty associated with $\Delta^{26}Mg_{Spl-Fo}$ is therefore also calculated by summing the uncertainties in quadrature. Finally, the temperature-dependent values of $\Delta^{26}Mg_{\text{mineral a–mineral b}}$ were regressed against $1/T^2$ by forcing the intercept through the origin using a York regression (Mahon, 1996) in order to obtain equations for the temperature dependencies of $\Delta^{26}Mg_{Fo-Mgs}$, $\Delta^{26}Mg_{Spl-Mgs}$, and $\Delta^{26}Mg_{Spl-Fo}$ with associated uncertainties.

3. RESULTS

Starting compositions of spinel, forsterite, and magnesite for each temperature are given in Table 1. Spinel–magnesite and forsterite–magnesite exchange experiments were conducted at 600, 700 and 800 °C at 10 kbar. Results are given in Table 2.

3.1. Textural evidence of exchange mechanism

Before considering the results of the experiments, it is instructive to examine possible mechanisms of exchange responsible for the isotopic evolution observed in the experiments. Fig. 2 is a series of scanning electron microscope (SEM) backscattered electron images of the forsterite starting material and forsterite–magnesite run products. The synthetic forsterite starting material (before powdering) consists of subhedral crystals ranging in size from sub-micron up to ~50 μm grains (Fig. 2a). Run products from an 800 °C Fo–Mgs run are shown in Fig. 2b. After the magnesite has been removed from the run products by preferential dissolution, evidence of reaction between forsterite and magnesite at high P–T is revealed in the form of dissolution/recrystallization textures (step-wise growth on crystal faces) exhibited by forsterite grains (Fig. 2c). Based on these textural observations and the anhydrous nature of the present experiments, we suggest that the mechanism of chemical and isotopic change may be annealing and recrystallization at high temperature and pressure (e.g., Griggs et al., 1960; Chiba et al., 1989; Clayton et al., 1989). Similar evidence for grain growth was observed in Spl–Mgs experiments, suggesting a similar exchange mechanism.

3.2. Forsterite–magnesite experiments

Mg isotope exchange experiments involving forsterite and magnesite were performed at 10 kbar and 800 °C (Fig. 3a and b) for 15, 30, 60, and 120 min, 700 °C (Fig. 3c and d) for 15, 30, and 60 min, and at 600 °C

Table 2
Experimental results. δ values are reported relative to Spex 3 for 700 °C experiments, and Spex 4 for 600 and 800 °C experiments.

Temp. (°C)	Run	Time (min)	Mineral	δ^{25}Mg (‰)	2se	δ^{26}Mg (‰)	2se
600	Sp516121	240	Spinel	−10.672	0.012	−10.898	0.016
600	Sp516122	60	Spinel	−11.282	0.006	−11.616	0.022
600	Sp516123	120	Spinel	−11.213	0.010	−11.517	0.020
600	Sp516121	240	Magnesite	0.446	0.014	1.809	0.022
600	Sp516122	60	Magnesite	1.015	0.010	2.455	0.018
600	Sp516123	120	Magnesite	1.199	0.012	2.653	0.010
600	Fo516121	240	Forsterite	−10.315	0.018	−10.352	0.010
600	Fo516122	60	Forsterite	−10.216	0.012	−10.192	0.016
600	Fo516123	120	Forsterite	−10.533	0.018	−10.594	0.018
600	Fo516121	240	Magnesite	−1.160	0.014	0.000	0.014
600	Fo516122	60	Magnesite	−1.333	0.010	−0.154	0.008
600	Fo516123	120	Magnesite	−1.531	0.014	−0.293	0.016
700	Sp713111	15	Spinel	−9.153	0.032	−9.641	0.024
700	Sp713112	30	Spinel	−10.011	0.074	−10.661	0.010
700	Sp713113	60	Spinel	−12.238	0.034	−13.214	0.026
700	Sp713111	15	Magnesite	−0.860	0.014	−0.310	0.010
700	Sp713112	30	Magnesite	0.067	0.026	0.742	0.026
700	Sp713113	60	Magnesite	0.247	0.030	0.963	0.022
700	Fo713111	15	Forsterite	−7.810	0.008	−8.072	0.022
700	Fo713112	30	Forsterite	−8.005	0.005	−8.371	0.008
700	Fo713113	60	Forsterite	−7.237	0.035	−7.441	0.018
700	Fo713111	15	Magnesite	−1.479	0.012	−0.889	0.014
700	Fo713112	30	Magnesite	−1.372	0.006	−0.750	0.009
700	Fo713113	60	Magnesite	−1.674	0.016	−1.110	0.018
800	Sp517122	120	Spinel	−10.577	0.030	−10.810	0.035
800	Sp518121	60	Spinel	−10.752	0.042	−11.060	0.096
800	Sp51122	30	Spinel	−10.190	0.042	−10.341	0.024
800	Sp1014111	15	Spinel	−11.208	0.006	−11.459	0.035
800	Sp1018111	30	Spinel	−11.067	0.010	−11.323	0.010
800	Sp1018112	60	Spinel	−10.845	0.004	−11.048	0.090
800	Sp517122	120	Magnesite	−0.097	0.026	1.309	0.050
800	Sp518121	60	Magnesite	−0.560	0.044	0.783	0.034
800	Sp51122	30	Magnesite	0.204	0.034	1.577	0.057
800	Sp1014111	15	Magnesite	0.562	0.010	1.981	0.022
800	Sp1018111	30	Magnesite	0.282	0.021	1.645	0.026
800	Sp1018112	60	Magnesite	0.206	0.020	1.565	0.016
800	Fo517122	120	Forsterite	−6.714	0.013	−6.284	0.016
800	Fo518121	60	Forsterite	−8.931	0.012	−8.825	0.020
800	Fo51122	30	Forsterite	−8.762	0.015	−8.634	0.042
800	Fo1014111	15	Forsterite	−7.767	0.013	−7.448	0.010
800	Fo1018111	30	Forsterite	−7.335	0.010	−6.974	0.010
800	Fo1018112	60	Forsterite	−8.502	0.006	−8.277	0.008
800	Fo517122	120	Magnesite	−3.034	0.010	−2.087	0.012
800	Fo518121	60	Magnesite	−2.113	0.013	−1.050	0.018
800	Fo51122	30	Magnesite	−2.031	0.012	−0.960	0.014
800	Fo1014111	15	Magnesite	−1.591	0.022	−0.429	0.055
800	Fo1018111	30	Magnesite	−2.178	0.016	−1.113	0.026
800	Fo1018112	60	Magnesite	−1.956	0.022	−0.881	0.037

(Fig. 3e and f) for 60, 120, and 240 min. None of these experiments attained isotopic equilibrium, as indicated by the fact that none of the experimental run products have compositions on the secondary fractionation lines. The equilibrium Mg isotope ratios of forsterite and magnesite were therefore obtained by extrapolation to the respective SFLs. The validity of linear extrapolation to the SFL has been investigated and verified by Lazar et al. (2012). Extrapolation of the regressed data to the SFLs at each temperature yielded $\Delta^{26}Mg_{Fo-Mgs}$ values of 0.04 ± 0.04‰ at 800 °C, 0.11 ± 0.10‰ at 700 °C, and 0.44 ± 0.10‰ at 600 °C.

3.3. Spinel–magnesite experiments

Experiments between spinel and magnesite were performed in tandem with and for the same durations as the Fo–Mgs experiments, at 10 kbar and 800 °C (Fig. 4a and b), 700 °C (Fig. 4c and d), and 600 °C (Fig. 4e and f). As

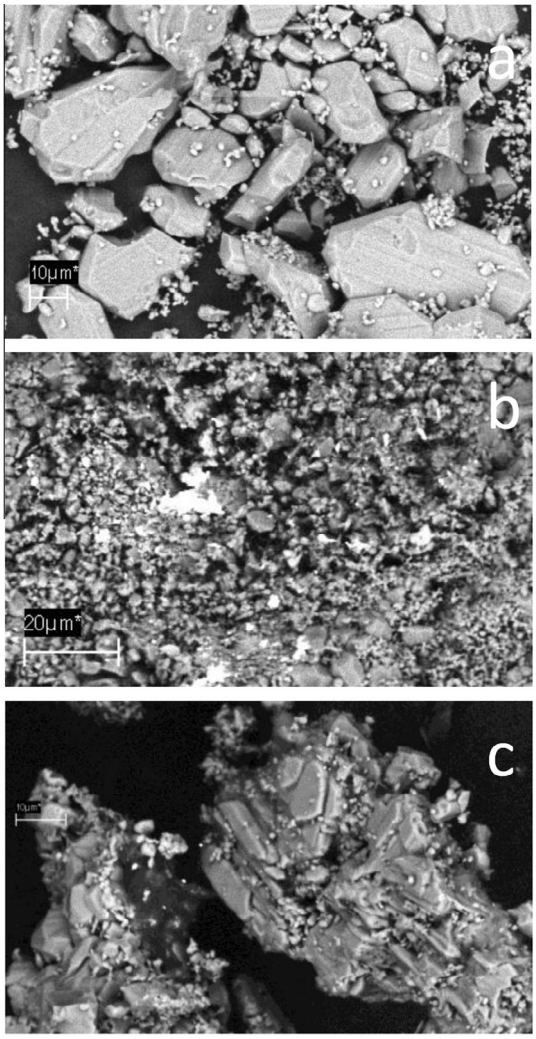

Fig. 2. SEM photomicrographs of (a) forsterite starting material before grinding, (b) forsterite + magnesite after run, and (c) forsterite after preferential dissolution of magnesite after run. The textures in (c) show clear evidence of dissolution and recrystallization in the form of step-like features diagnostic of reprecipitation.

with the Fo–Mgs experiments, none of these experiments attained isotopic equilibrium. Therefore the equilibrium Mg isotope ratios of spinel and magnesite at each temperature were also obtained by linear extrapolation to the respective SFLs. Extrapolation of the regressed data to the SFLs at each temperature yielded $\Delta^{26}Mg_{Spl-Mgs}$ values of $0.90 \pm 0.28‰$ at 800 °C, $1.10 \pm 0.27‰$ at 700 °C, and $1.73 \pm 0.38‰$ at 600 °C.

3.4. Spinel–forsterite fractionation by difference

From the experimentally determined equilibrium fractionation values for forsterite–magnesite and spinel–magnesite, we determine equilibrium fractionation between spinel and forsterite by difference. This yielded $\Delta^{26}Mg_{Spl-Fo}$ values of $0.86 \pm 0.29‰$ at 800 °C, $0.99 \pm 0.29‰$ at 700 °C, and $1.29 \pm 0.39‰$ at 600 °C.

3.5. Temperature dependence of equilibrium Mg isotope exchange

The experimentally determined Fo–Mgs and Spl–Mgs fractionations are plotted as a function of temperature in Fig. 5a and b, along with theoretical lines for forsterite and spinel equilibrium fractionation with magnesite from Schauble (2011). Regressing these data by forcing the best-fit lines through the origin leads to equations for the temperature dependence of the Fo–Mgs and Spl–Mgs fractionation factors:

$$\Delta^{26}Mg_{Fo-Mgs} = 0.06(\pm 0.04) \times 10^6/T^2 \quad (6)$$

$$\Delta^{26}Mg_{Spl-Mgs} = 1.04(\pm 0.20) \times 10^6/T^2 \quad (7)$$

where uncertainties reflect propagation of standard errors multiplied by 2 (propagation of 2se through the regressions). Using the differences between the experimentally determined forsterite–magnesite and spinel–magnesite fractionation at each temperature, we obtain an equation for the temperature dependence of the spinel–forsterite fractionation factor:

$$\Delta^{26}Mg_{Spl-Fo} = 0.96(\pm 0.21) \times 10^6/T^2 \quad (8)$$

Fig. 5c shows spinel–forsterite equilibrium fractionation as a function of temperature plotted together with a predicted fractionation based on *ab initio* density functional perturbation theory calculations from Schauble (2011).

4. DISCUSSION

4.1. Comparison to theoretical predictions

Recent theoretical studies have predicted the magnitude and direction of magnesium isotope fractionation between various phases and molecules at a range of temperatures and pressures (Black et al., 2007; Rustad et al., 2010; Schauble, 2011). Of these, only Schauble (2011) reported theoretical calculations of equilibrium magnesium isotope fractionation between Mg-bearing oxides, silicates, and carbonates. We compare our experimentally determined equilibrium fractionation factors (expressed as $\Delta^{26}Mg_{Fo-Mgs}$, $\Delta^{26}Mg_{Spl-Mgs}$ and $\Delta^{26}Mg_{Spl-Fo}$) with those predicted by Schauble (2011) in Fig. 5a–c.

Mass-dependent equilibrium stable isotope fractionation is driven by changes in vibrational energies in crystals due to isotopic substitution (e.g., Urey, 1947; Bigeleisen and Mayer, 1947). Schauble (2011) used density functional perturbation theory (DFPT) to calculate vibrational frequencies in magnesium-bearing crystals, allowing for the calculation of associated mass-dependent shifts in frequencies with isotope substitution. The calculations by Schauble (2011) suggest that inter-mineral Mg isotope fractionations should be measurable over a range of temperatures, with values ranging from several per mil at room temperature to several tenths of per mil at igneous and metamorphic temperatures. This work predicts that spinel will have higher $^{26}Mg/^{24}Mg$ than typical coexisting silicate phases (e.g., $\Delta^{26}Mg_{Spl-Fo} = 0.59$ at 1000 °C), while carbonates will have low $^{26}Mg/^{24}Mg$ with respect to spinel and silicates, the

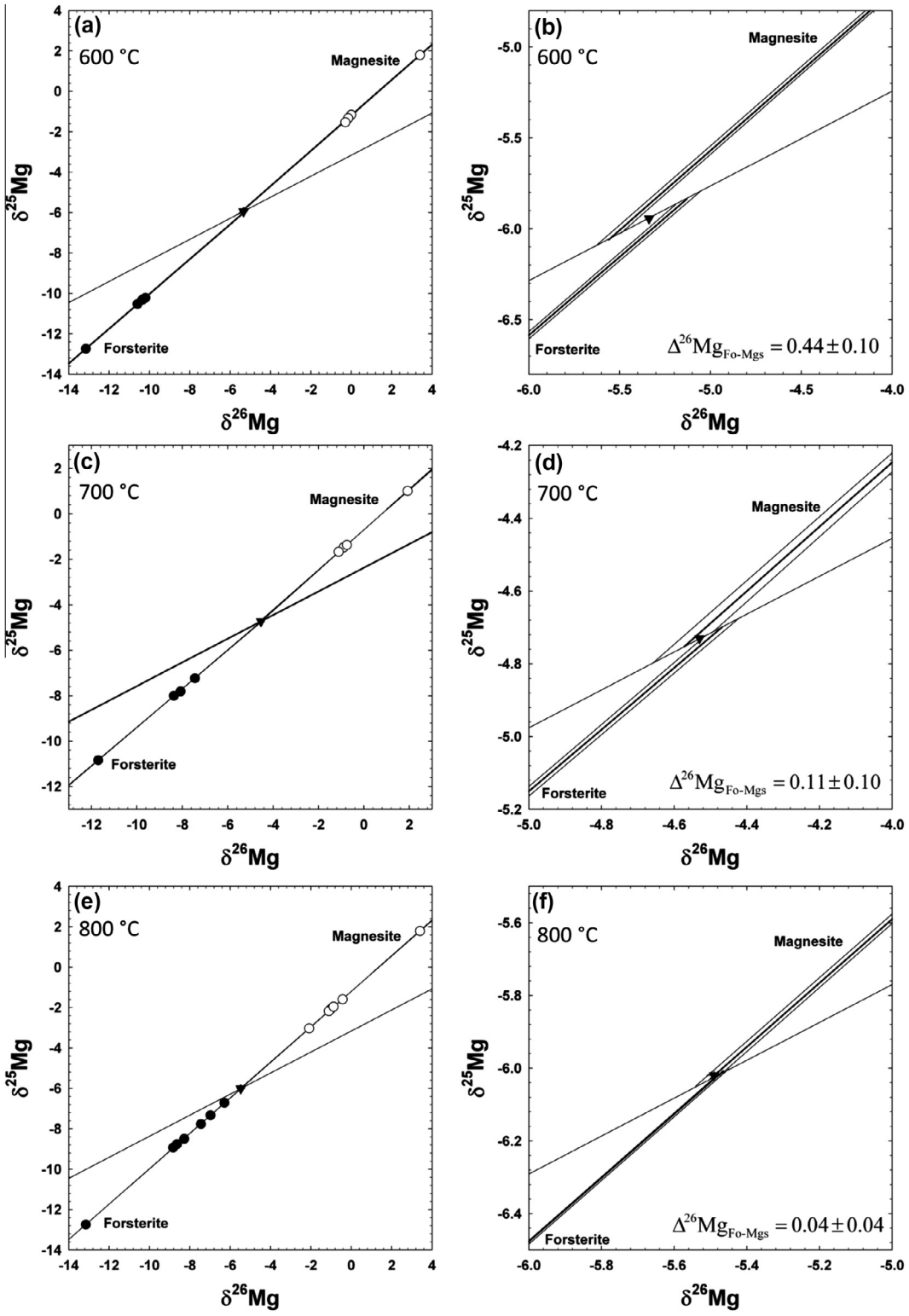

Fig. 3. Experimental results for magnesite and forsterite at 600 °C (a and b), 700 °C (c and d), and 800 °C (e and f). Panels b, d, and f are close-ups of a, c, and e, respectively. The open circles are magnesite, closed circles are forsterite, and upside down triangles are bulk compositions measured directly for all cases except for Fo–Mgs 700 °C, where the bulk was calculated from starting compositions. Error bars (2se) are shown where they are larger than symbols. Heavy lines going through experimental data are best-fit lines calculated using a York regression (Mahon, 1996). Thinner lines on either side of best-fit lines are 2se error envelopes.

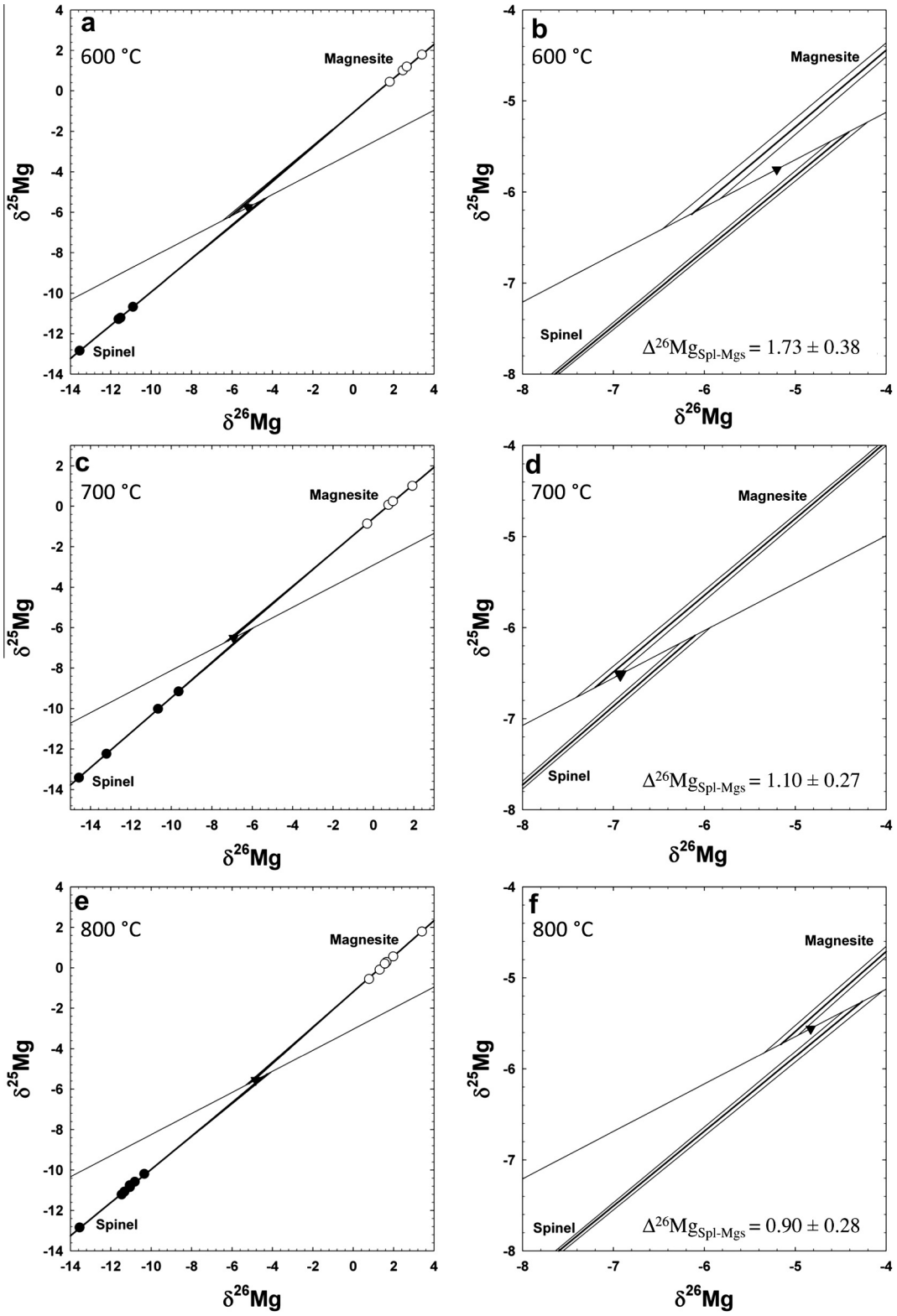

Fig. 4. Experimental results for spinel and magnesite at 600 °C (a and b), 700 °C (c and d), and 800 °C (e and f). Fig. 4b, d, and f are close-ups of a, c, and e, respectively. The open circles are magnesite, closed circles are spinel, and upside down triangles are measured bulk compositions. Error bars (2se) are shown where they are larger than symbols. Heavy lines going through experimental data are best-fit lines calculated using a York regression (Mahon, 1996). Thinner lines on either side of best-fit lines are 2se error envelopes.

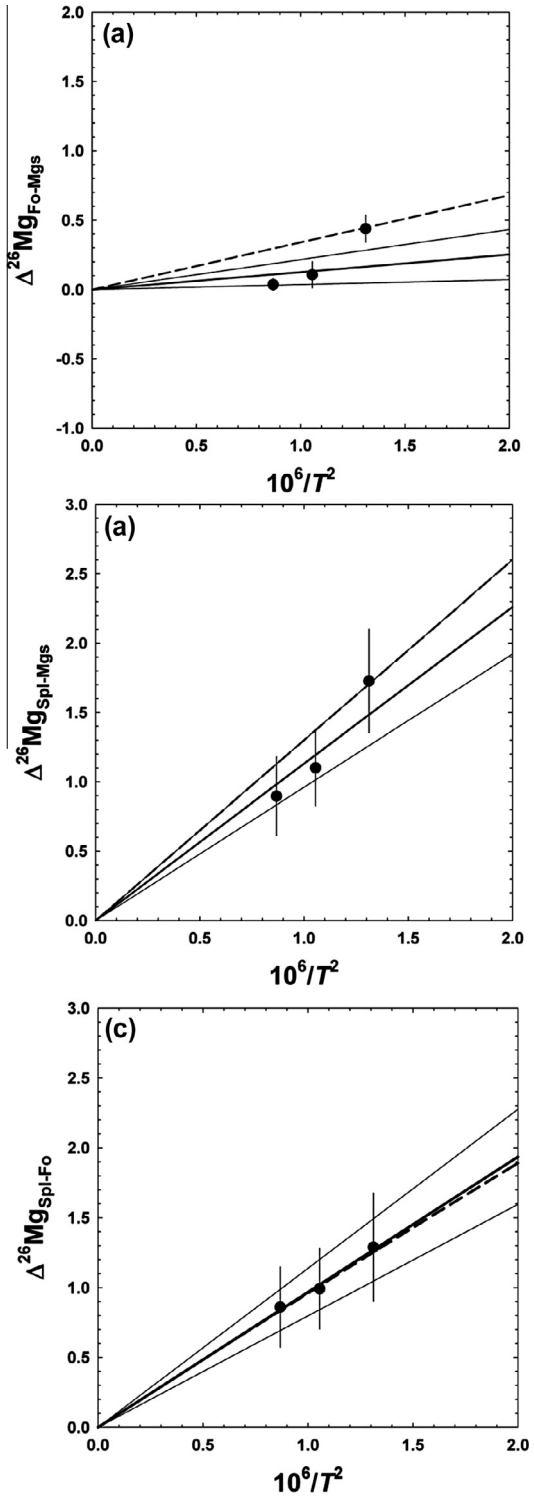

Fig. 5. Experimental forsterite–magnesite (a), spinel–magnesite (b), and spinel–forsterite (c) Mg isotope fractionation data plotted as a function of temperature along with theoretical predictions (see text). Heavy lines are linear best-fits through the data (forced through the origin), thin lines are error envelopes representing propagation of 2se analytical errors, and dashed lines are theoretical predictions (Schauble, 2011). Error bars for the data are 2se.

affinity for the heavy isotopes correlating inversely with coordination number.

In the case of both forsterite–magnesite (Fig. 5a) and spinel–magnesite (Fig. 5b), our experimentally determined Δ vs. $1/T^2$ relationships have shallower slopes than the theoretically predicted values. Note that in both instances, the 600 °C data lie directly on the theoretical line, whereas the data for 700 and 800 °C lie at lower Δ values. The observed discrepancies could be due to experimental and/or analytical error in one or more sets of experiments involving magnesite in this study, although we have no reason to believe that the 600 °C data are any more accurate than the higher temperature data. In fact, in both sets of 600 °C experiments, the run products were the less equilibrated than in the respective 700 and 800 °C series, requiring greater extrapolation to equilibrium values, and therefore higher degrees of uncertainty. Alternatively, errors related to the theoretical calculations, or some combination of theoretical, experimental, analytical error, could be the cause of the observed discrepancies.

The spinel–forsterite fractionation factor determined by this study agrees with theoretical predictions within analytical uncertainties (Fig. 5c). Because the spinel–forsterite fractionation factor was determined by the difference between the spinel–magnesite and forsterite–magnesite fractionations at each temperature, discrepancies between our carbonate-mineral fractionations and those predicted by theory discussed above cancel in the derived relationship between $\Delta^{26}Mg_{Spl-Fo}$ and temperature.

4.2. Spinel–olivine Mg isotope geothermometry

Several studies report small but resolvable inter-mineral $^{26}Mg/^{24}Mg$ isotope fractionation (up to ~0.4‰) between coexisting pyroxene and olivine in mantle rocks (e.g., Wiechert and Halliday, 2007; Handler et al., 2009; Yang et al., 2009; Young et al., 2009; Liu et al., 2011). Only two investigations to date include measurements of Mg isotope fractionation between coexisting mantle spinel and olivine, those of Young et al. (2009) and Liu et al. (2011). Both studies found that in all cases in mantle xenoliths, spinel is higher in $^{26}Mg/^{24}Mg$ than coexisting olivine. Although the studies agree as to the direction of fractionation ($\Delta^{26}Mg_{Spl-Fo} > 0$), they report small but resolvable differences in the magnitude of fractionation. These small differences must be understood if Mg isotopes are to be used as a geothermometer or a tracer of mantle processes.

Fig. 6 shows spinel–olivine Mg isotope fractionation data from Young et al. (2009) and Liu et al. (2011), along with theoretically (Schauble, 2011) and experimentally (this study) determined fractionations for stoichiometric pure spinel ($MgAl_2O_4$) and forsterite as functions of temperature. Spinel–olivine data from Liu et al. (2011) fall below the theoretically predicted and experimentally determined pure Al–spinel–forsterite fractionation lines, while data from Young et al. (2009) agree, within error, with both. These apparent discrepancies could result from the use of different thermometers in the two studies. Liu et al. (2011)

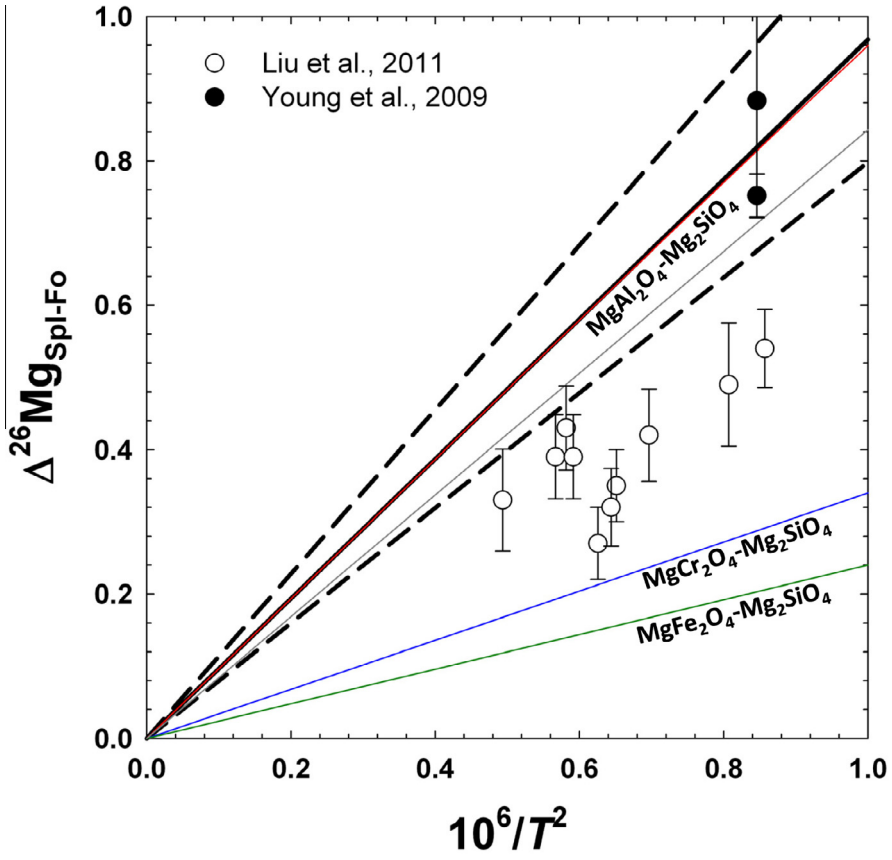

Fig. 6. Comparison of measured Spl–Ol Mg isotope fractionation (Young et al., 2009; Liu et al. 2011) with experimentally and theoretically determined fractionation as a function of temperature. The heavy black line is the experimentally derived Spl–Fo fractionation. Dashed lines represent 2se errors on the experimental best-fit line. Colored lines are from theoretical calculations by Schauble (2011) for Al–spinel–forsterite (red), magnesiochromite–forsterite (blue), and magnesioferrite–forsterite (green) fractionation. The experimental fractionation line and theoretical fractionation line for pure Al–spinel–forsterite overlap at high temperatures and are almost indistinguishable as shown. The gray line represents the fractionation line calculated by Liu et al. (2011) based on the Al:Cr:Fe^{3+} ratios of their spinels. Further discussion in text. (For interpretation of the references to color in this figure legend, the reader is referred to the web version of this article.)

use temperatures for Kuandian peridotites previously reported in Wu et al. (2006), which were calculated using the two-pyroxene Ca thermometer of Brey and Köhler (1990), but report no estimate of uncertainties. A comparison of calculated temperatures for the same Kuandian peridotites using several different pyroxene thermometers (see Electronic Annex EA-5 of Wu et al., 2006 and references therein), reveals a large range of equilibration temperatures from 528 to 1236 °C for the suite of peridotites. Conversely, Young et al. (2009) compared their Mg isotope fractionation factors to the temperature recorded by the inversion parameter for Mg–Al ordering in Type I San Carlos spinels (Uchida et al., 2005). The temperature implied by Mg isotope thermometry derived from density functional calculations of Schauble (2011) agree within error with the spinel ordering. Young et al. (2009) reported an average uncertainty of ±60 °C for two xenoliths.

Liu et al. (2011) proposed that the likely reason for disagreements between their data and theoretical predictions, is that spinels in mantle rocks are not endmember $MgAl_2O_4$. They conclude that the reason for the discrepancy between their data and expected values is the complicating effects of crystal chemical substitutions in spinels and the effects that these substitutions have on fractionation. Theory supports this interpretation qualitatively. Schauble (2011) calculates that Mg^{IV} isotope partitioning in normal spinel structures ($A^{IV}(B_2)^{VI}O_4$) depends strongly on the occupancy of the octahedral site (i.e., the identity of B^{3+}). Although this phenomenon is not fully understood, it appears that the affinity of the tetrahedral site for high $^{26}Mg/^{24}Mg$ is reduced by substitution of Cr or Fe^{3+} for Al on octahedral sites. Therefore, natural spinels with varying amounts of Al, Cr, and Fe^{3+} in the octahedral position will likely possess $\Delta^{26}Mg_{Spl-Fo}$ intermediate between values predicted for pure $MgAl_2O_4$ spinel–forsterite, and magnesiochromite–forsterite, or normal magnesioferrite–forsterite pairs. The effects of small inverse spinel components typical of mantle spinels on magnesium isotope partitioning are not known.

There is strong agreement between equilibrium $\Delta^{26}Mg_{Spl-Fo}$ values from the present work, which uses end-member synthetic $MgAl_2O_4$ spinel and forsterite, and those predicted by Schauble (2011) for pure spinel and forsterite, thus supporting the use of Mg isotopes in spinel and coexisting silicates as a geothermometer. However, since

natural samples are rarely end-member compositions, caution should be exercised when extracting temperatures based on Mg isotope ratios alone. In the study by Young et al. (2009), the Cr^{VI} and $(Fe^{3+})^{VI}$ contents of the spinels suggest that the measured spinel–forsterite fractionations are high compared with theory if the fractionation factors scale linearly with substitutions for Al^{VI}. If so, the agreement found by these authors between temperatures obtained from the Mg isotope ratios of spinels and olivines and those from spinel tetrahedral/octahedral ordering would be fortuitous. Until more experiments are performed with different spinel compositions, we must rely on interpolation of theoretical predictions (Schauble, 2011) for estimating the effects of cation substitutions on the affinity of spinel for the heavy isotopes of Mg. The present experiments anchor these estimates for the end-member normal $MgAl_2O_4$ component.

4.3. Magnesite in the mantle

Subducted oceanic crust contains significant amounts of carbonate (Alt and Teagle, 1999) not quantitatively removed by devolatilization reactions (Yaxley and Green, 1994; Molina and Poli, 2000; Kerrick and Connolly, 2001). High *T*–*P* experiments have shown that magnesite is a stable carbonate at mantle conditions (e.g., Biellmann et al., 1993). It therefore has the ability to store carbon in the Earth's mantle and is a carrier of carbon in subducting plates (Kushiro, 1975; Brey et al., 1983; Katsura et al., 1991; Biellmann et al., 1993; Gillet, 1993; Redfern et al., 1993; Zhang and Liou, 1994; Kelemen et al., 2011). While carbon isotopes are useful for identifying recycled organic carbonate, they are not very sensitive to inorganic carbonate due to the smaller fractionations involved (Yang et al., 2012). Therefore, magnesium isotopes are potentially powerful tracers of interactions between mantle rocks and recycled carbonate. The experimentally determined Mg-isotope fractionation between magnesite and spinel and magnesite and forsterite from the present study provide guidelines for interpreting the $\delta^{26}Mg$ signals of high *T*–*P* magnesite coexisting with silicates and oxides.

Magnesite occurs as an alteration product in Mg-rich igneous and metamorphic rocks. It has been observed in kimberlites, eclogites, and mantle peridotites (e.g., McGetchin and Besancon, 1973; Lappin and Smith, 1978; Yang et al., 1993; Zhang and Liou, 1994). Yang et al. (1993) reported magnesite-bearing garnet peridotite consisting of garnet + forsterite + enstatite + diopside + magnesite. They found magnesite occurring as interstitial grains between olivine crystals and showing textural evidence of equilibrium with olivine. Such assemblages would be ideal for Mg-isotopic analysis and interpretation using the results of this study. Our experiments lead to the prediction that, at equilibrium magnesite should preferentially fractionate light Mg isotopes relative to both spinel and olivine. An equilibrium assemblage of spinel + forsterite + magnesite would yield Mg isotope values of $\delta Mg_{Spl} \gg \delta Mg_{Fo} > \Delta Mg_{Mgs}$. There is a relatively large Mg isotope fractionation between spinel and magnesite and between spinel and forsterite due to the differences in coordination of Mg in spinel (tetrahedral), and both forsterite and magnesite (octahedral), but a much smaller fractionation between forsterite and magnesite. Unfortunately, there are no existing Mg isotope data for coexisting magnesite–forsterite or magnesite–spinel to compare with the findings of the present study. In the future, experimentally determined $\Delta^{26}Mg_{Fo-Mgs}$ and $\Delta^{26}Mg_{Spl-Mgs}$ values given here will serve as a useful tool for determining the degree of equilibrium between olivine, magnesite, and spinel in naturally occurring igneous and metamorphic rocks such as those described above.

5. CONCLUSIONS

This study makes use of the three-isotope exchange method to determine experimentally the equilibrium magnesium isotope fractionation factors between forsterite and magnesite, and between spinel and magnesite, as a function of temperature. By using carbonate as both exchange medium and exchange partner, we successfully achieved significant exchange of Mg isotopes between the two mineral pairs at 600, 700, and 800 °C. These experiments in turn allow for the determination of the equilibrium fractionation between spinel and forsterite. Comparisons of experimental results reported here with theoretical predictions reveals close agreement for spinel–olivine fractionation, but some discrepancies between experiments and theory for forsterite–magnesite and spinel–magnesite fractionation are evident and warrant further investigation. In both cases involving carbonate, the experimentally determined values ($\Delta^{26}Mg_{Fo-Mgs}$ and $\Delta^{26}Mg_{Spl-Mgs}$) are lower than those predicted by theoretical calculations but agree in terms of the direction of fractionations. Results of these experiments provide a foundation for using Mg isotopes as tracers in mantle rocks. Further experiments are required to explore the effects of cation substitutions on Mg isotope fractionation at high temperatures in order to use Mg isotopes as a geothermometer for the natural range of peridotite compositions.

ACKNOWLEDGMENTS

We express thanks to Edwin Schauble for helpful discussions on equilibrium stable isotope fractionation theory, useful experimental ideas, and insightful comments on the manuscript. Adam Makhluf and Michael Huh are thanked for their assistance in the laboratory. Constructive comments from Fangzhen Teng, Ralph Dohmen, and an anonymous reviewer are greatly appreciated. We acknowledge support from National Science Foundation Grant EAR0711411 to E.D.Y., C.E.M., and E.S.

REFERENCES

Alt J. C. and Teagle D. A. H. (1999) The uptake of carbon during alteration of oceanic crust. *Geochim. Cosmochim. Acta* **63**, 1527–1535.

Biellmann C., Gillet P., Guyot F., Peyronneau J. and Reynard B. (1993) Experimental evidence for carbonate stability in the Earth's lower mantle. *Earth Planet. Sci. Lett.* **118**, 31–41.

Bigeleisen J. and Mayer M. G. (1947) Calculation of equilibrium constants for isotopic exchange reactions. *J. Chem. Phys.* **15**, 261–267.

Black J. R., Yin Q.-Z., Rustad J. R. and Casey W. H. (2007) Magnesium isotopic equilibrium in chlorophylls. *J. Am. Chem. Soc.* **129**, 8690–8691.

Brey G., Brice W. R., Ellis D. J., Green D. H., Harris K. L. and Ryabchikov I. D. (1983) Pyroxene–carbonate reactions in the upper mantle. *Earth Planet. Sci. Lett.* **62**, 63–74.

Brey G. P. and Köhler T. (1990) Geothermobarometry in four-phase lherzolites: II. New thermobarometers, and practical assessment of existing thermobarometers. *J. Petrol.* **31**, 1353–1378.

Chacko T., Hu X., Mayeda T. K., Clayton R. N. and Goldsmith J. R. (1996) Oxygen isotope fractionations in muscovite, phlogopite, and rutile. *Geochim. Cosmochim. Acta* **60**, 2595–2608.

Chakrabati R. and Jacobsen S. B. (2010) The isotopic composition of magnesium in the inner solar system. *Earth Planet. Sci. Lett.* **293**, 349–358.

Chiba H., Chacko T., Clayton R. N. and Goldsmith J. R. (1989) Oxygen isotope fractionations involving diopside, forsterite, magnetite, and calcite: Application to geothermometry. *Geochim. Cosmochim. Acta* **53**, 2985–2995.

Clayton R. N., Goldsmith J. R. and Mayeda T. K. (1989) Oxygen isotope fractionation in quartz, albite, anorthite, and calcite. *Geochim. Cosmochim. Acta* **53**, 725–733.

Galy A., Bar-Matthews M., Halicz L. and O'Nions R. K. (2002) Mg isotopic composition of carbonate: insight from speleothem formation. *Earth Planet. Sci. Lett.* **201**, 105–115.

Gillet P. (1993) Stability of magnesite ($MgCO_3$) at mantle pressure and temperature conditions: a Raman spectroscopic study. *Am. Mineral.* **78**, 1328–1331.

Griggs D. T., Paterson M. S., Heard H. C. and Turner F. J. (1960) Annealing recrystallization in calcite crystals and aggregates. *Geol. Soc. Am. Mem* **79**, 21–37.

Handler M. R., Baker J. A., Schiller M., Bennett V. C. and Yaxley G. M. (2009) Magnesium stable isotope composition of Earth's upper mantle. *Earth Planet. Sci. Lett.* **282**, 306–313.

Huang F., Zhang Z., Lundstrom C. C. and Zhi X. (2011) Iron and magnesium isotopic compositions of peridotite xenoliths from Eastern China. *Geochim. Cosmochim. Acta* **75**, 3318–3334.

Katsura T. and Ito E. (1990) Melting and subsolidus phase relations in the $MgSiO_3$–$MgCO_3$ system at high pressures: implications to evolution of the Earth's atmosphere. *Earth Planet. Sci. Lett.* **99**, 110–117.

Katsura T., Tsuchida Y., Ito E., Yagi T., Utsumi W. and Akimoto S. I. (1991) Stability of magnesite under the lower mantle conditions. *Proc. Jpn. Acad. B: Phys. Biol. Sci.* **67**, 57–60.

Kelemen P. B., Matter J., Streit E. E., Rudge J. F., Curry W. B. and Blusztajn J. (2011) Rates and mechanisms of mineral carbonation in peridotite: natural processes and recipes for enhanced, in situ CO_2 capture and storage. *Annu. Rev. Earth Planet. Sci.* **39**, 545–576.

Kerrick D. M. and Connolly J. A. D. (2001) Metamorphic devolatilization of subducted oceanic metabasalts: implications for seismicity, arc magmatism and volatile recycling. *Earth Planet. Sci. Lett.* **189**, 19–29.

Kushiro I. (1975) Carbonate–silicate reactions at high pressures and possible presence of dolomite and magnesite in the upper mantle. *Earth Planet. Sci. Lett.* **28**, 116–120.

Lappin M. A. and Smith D. C. (1978) Mantle-equilibrated orthopyroxene eclogite pods from the basal gneisses in the Selje District, Western Norway. *J. Petrol.* **19**, 530–584.

Lazar C., Young E. D. and Manning C. E. (2012) Experimental determination of equilibrium nickel isotope fractionation between metal and silicate from 500 °C to 950 °C. *Geochim. Cosmochim. Acta* **86**, 276–295.

Liu S. A., Teng F. Z., Yang W. and Wu F. Y. (2011) High-temperature inter-mineral magnesium isotope fractionation in mantle xenoliths from the North China craton. *Earth Planet. Sci. Lett.* **308**, 131–140.

Mahon K. I. (1996) The New "York" regression: application of an improved statistical method to geochemistry. *Int. Geol. Rev.* **38**, 293–303.

Manning C. E. and Boettcher S. L. (1994) Rapid-quench hydrothermal experiments at mantle pressures and temperatures. *Am. Mineral.* **79**, 1153–1158.

Matsuhisa Y., Goldsmith J. R. and Clayton R. N. (1978) Mechanisms of hydrothermal crystallization of quartz at 250 °C and 15 kbar. *Geochim. Cosmochim. Acta* **42**, 173–182.

Mavromatis V., Pearce C. R., Shirokova L. S., Bundeleva A., Pokrovsky O. S., Benezeth P. and Oelkers E. H. (2011) Magnesium isotope fractionation during hydrous magnesium carbonate precipitation with and without cyanobacteria. *Geochim. Cosmochim. Acta* **76**, 161–174.

McGetchin T. R. and Besancon J. R. (1973) Carbonate inclusions in mantle-derived pyropes. *Earth Planet. Sci. Lett.* **18**, 408–410.

Molina J. F. and Poli S. (2000) Carbonate stability and fluid composition in subducted oceanic crust: an experimental study on H_2O–CO_2 bearing basalts. *Earth Planet. Sci. Lett.* **176**, 295–310.

Pearce C. R., Saldi G. D., Schott J. and Oelkers E. H. (2012) Isotopic fractionation during congruent dissolution, precipitation and at equilibrium: evidence from Mg isotopes. *Geochim. Cosmochim. Acta* **92**, 170–183.

Redfern S. A. T., Wood B. J. and Henderson C. M. B. (1993) Static compressibility of magnesite to 20 GPa: implications for $MgCO_3$ in the lower mantle. *Geophys. Res. Lett.* **20**, 2099–2102.

Rustad J. R., Casey W. H., Yin Q. Z., Bylaska E. J., Felmy A. R., Bogatko S. A., Jackson V. E. and Dixon D. A. (2010) Isotopic fractionation of Mg^{2+} (aq), Ca^{2+} (aq), and Fe^{2+} (aq) with carbonate minerals. *Geochim. Cosmochim. Acta* **74**, 6301–6323.

Shahar A., Young E. D. and Manning C. E. (2008) Equilibrium high-temperature Fe isotope fractionation between fayalite and magnetite: an experimental calibration. *Earth Planet. Sci. Lett.* **268**, 330–338.

Shahar A., Ziegler K., Young E. D., Ricolleau A., Schauble E. A. and Fei Y. (2009) Experimentally determined Si isotope fractionation between silicate and metal and implications for Earth's core formation. *Earth Plant. Sci. Lett.* **288**, 228–234.

Shahar A., Hillgren V. J., Young E. D., Fei Y., Macris C. and Deng L. (2011) High-temperature Si isotope fractionation between iron metal and silicate. *Geochim. Cosmochim. Acta* **75**, 7688–7697.

Schauble E. A. (2011) First-principles estimates of equilibrium magnesium isotope fractionation in silicate, oxide, carbonate and hexaaquamagnesium (2+) crystals. *Geochim. Cosmochim. Acta* **75**, 844–869.

Uchida H., Lavina B., Downs R. T. and Chesley J. (2005) Single crystal X-ray diffraction of spinels from the San Carlos volcanic field, Arizona: spinel as a geothermometer. *Am. Mineral.* **90**, 1900–1908.

Ulmer G. C. (1971) *Research Techniques for High Pressure and High Temperature*. Springer-Verlag.

Urey H. C. (1947) The thermodynamic properties of isotopic substances. *J. Chem. Soc.*, 562–581.

Wiechert U. and Halliday A. N. (2007) Non-chondritic magnesium and the origins of the inner terrestrial planets. *Earth Planet. Sci. Lett.* **256**, 360–371.

Williams H. M., Nielsen S. G., Renac C., Griffin W. L., O'Reilly S. Y., McCammon C. A., Pearson N., Viljoen F., Alt J. C. and Halliday A. N. (2009) Fractionation of oxygen and iron isotopes by partial melting processes: implications for the interpretation of stable isotope signatures in mafic rocks. *Earth Planet. Sci. Lett.* **283**, 156–166.

Wombacher F., Eisenhauer A., Böhm F., Gussone N., Kinkel H., Lezius J., Noe S., Regenberg M. and Rüggeberg A. (2006) Magnesium stable isotope compositions in biogenic $CaCO_3$. *Geophys. Res. Abstr.* **8**, 06353.

Wu F.-Y., Walker R. J., Yang Y.-H., Yuan H.-L. and Yang J.-H. (2006) The chemical–temporal evolution of lithospheric mantle underlying the North China craton. *Geochim. Cosmochim. Acta* **70**, 5013–5034.

Yang J., Godard G., Kienast J. R., Lu Y. and Sun J. (1993) Ultrahigh-pressure (60 kbar) magnesite-bearing garnet peridotites from northeastern Jiangsu, China. *J. Geol.* **101**, 541–554.

Yang W., Teng F. Z. and Zhang H. F. (2009) Chondritic magnesium isotopic composition of the terrestrial mantle: a case study of peridotite xenoliths from the North China craton. *Earth Planet. Sci. Lett.* **288**, 475–482.

Yang W., Teng F. Z., Zhang H. F. and Li S. G. (2012) Magnesium isotopic systematics of continental basalts from the North China craton: implications for tracing subducted carbonate in the mantle. *Chem. Geol.* **328**, 185–194.

Yaxley G. M. and Green D. H. (1994) Experimental demonstration of refractory carbonate-bearing eclogite and siliceous melt in the subduction regime. *Earth Planet. Sci. Lett.* **128**, 313–325.

Young E. D. and Galy A. (2004) The isotope geochemistry and cosmochemistry of magnesium. *Rev. Mineral. Geochem.* **55**, 197–230.

Young E. D., Tonui E., Manning C. E., Schauble E. and Macris C. A. (2009) Spinel–olivine magnesium isotope thermometry in the mantle and implications for the Mg isotopic composition of Earth. *Earth Planet. Sci. Lett.* **288**, 524–533.

Zhang R. Y. and Liou J. G. (1994) Coesite-bearing eclogite in Henan Province, central China: detailed petrography, glaucophane stability and PT-path. *Eur. J. Mineral.* **6**, 217–233.

Associate editor: Stefan Weyer